

## Synthesis and characterization of strontium aluminate based on utilizing alum sludge

R.M. Khattab\*, F. Abd-EL-Raouf, H.E.H. Sadek, A.A. Gaber

Refractories, Ceramics and Building Materials Department, National Research Centre (NRC), Dokki, 12622 Cairo, Egypt, Tel. +20 1015892223; emails: rihamkhattab78@yahoo.com (R.M. Khattab), f1abdelraouf@gmail.com (F. Abd-EL-Raouf), hsadek2004@yahoo.com (H.E.H. Sadek), amany1gaber@yahoo.com (A.A. Gaber)

Received 4 November 2018; Accepted 17 February 2019

### ABSTRACT

The aim of this work is recycling the alum sludge to produce valuable strontium aluminate ( $\text{SrAl}_2\text{O}_4$ ) materials.  $\text{Sr}(\text{NO}_3)_2$  is used as starting material beside alum sludge. The alum sludge was treated with a suitable chemical method and followed by thermal treatment at  $1,400^\circ\text{C}$  for alpha alumina production. Part of  $\text{Sr}(\text{NO}_3)_2$  powders were calcined at  $1,100^\circ\text{C}$  at different heating rates and times to obtain  $\text{Sr}(\text{OH})_2$ ,  $\text{Sr}(\text{OH})_2\text{OH}$ , or  $\text{SrO}$  powders. Four compositions were prepared based on the addition of  $\text{Sr}(\text{NO}_3)_2$ ,  $\text{Sr}(\text{OH})_2$ ,  $\text{Sr}(\text{OH})_2\text{OH}$ , or  $\text{SrO}$  powders with alumina for  $\text{SrAl}_2\text{O}_4$  formation and calcined at  $1,100^\circ\text{C}$ . The calcined powders were compacted and sintered at different temperatures:  $1,200^\circ\text{C}$ ,  $1,400^\circ\text{C}$  and  $1,500^\circ\text{C}$  to follow the phase composition. The optimum composition was sintered at  $1,550^\circ\text{C}$  and  $1,650^\circ\text{C}$ . Phase composition of sintered batches was determined by XRD. The particle morphology of the sintered samples was estimated by SEM. Apparent porosity, bulk density and compressive strength for sintered batches were investigated. Batch compositions containing  $\text{SrO}$  gave a high yield of  $\text{SrAl}_2\text{O}_4$  accompanied by an improvement in the physical and mechanical properties after sintering at  $1,550^\circ\text{C}$ .

*Keywords:* Strontium aluminate; Alum sludge; Sintering; Alpha alumina; Phase composition

### 1. Introduction

The alum sludge is a good source for aluminum compounds,  $\text{SiO}_2$  and  $\text{Fe}_2\text{O}_3$ . Therefore, many efforts have been made to recycle the alum sludge [1–3]. It can be used for producing value-added products such as aluminum hydroxide  $\text{Al}(\text{OH})_3$  [2], which is very attractive to be calcined to produce aluminum oxide products.

In the  $\text{SrO}-\text{Al}_2\text{O}_3$  system [4], there are five well-known stable double oxides (binary phases) namely;  $\text{Sr}_4\text{Al}_2\text{O}_7$  (tetrastrontium aluminate,  $\text{Sr}_4\text{A}$ ),  $\text{Sr}_3\text{Al}_2\text{O}_6$  (cubic tri-strontium aluminate,  $\text{Sr}_3\text{A}$ ),  $\text{SrAl}_2\text{O}_4$  (monoclinic strontium aluminate,  $\text{SrA}$ ),  $\text{SrAl}_4\text{O}_7$  (strontium di-aluminate,  $\text{SrA}_2$ ),  $\text{SrAl}_{12}\text{O}_{19}$  (hexagonal strontium hexa aluminate,  $\text{SrA}_6$ ) [5] and other strontium aluminate phases, such as  $\text{Sr}_4\text{Al}_{14}\text{O}_{25}$  (orthorhombic),

$\text{Sr}_{12}\text{Al}_{14}\text{O}_{33}$  and  $\text{Sr}_{10}\text{Al}_6\text{O}_{19}$  as described in the literature [6]. Strontium aluminates have a vital utilization as aluminous hydraulic binder materials as special inorganic cements possess the properties, which make it suitable for different special uses or applications such as macro defect free composites, blended as well as expansive cements for high temperature applications “cement installations”, household goods, road surfaces, and were used in the disposal for nuclear or radioactive wastes [3,5,7–9]. Moreover, strontium aluminate can be used as phosphorescent-based purposes or thermoluminescent pigments, anodes for oxide fuel cells and highly conductive electrolytes [10,11]. The most commonly used strontium aluminate hosts are  $\text{SrAl}_2\text{O}_4$  and  $\text{Sr}_4\text{Al}_{14}\text{O}_{25}$  and most publications on strontium aluminate phases are related to the strong green emission (~530 nm) of  $\text{Eu}^{2+}$  in stoichiometric  $\text{SrAl}_2\text{O}_4$  with monoclinic tridymite structure [12–15].  $\text{SrAl}_2\text{O}_4$  has been proven to be an efficient host material for

\* Corresponding author.

photoluminescence (PL), cathodoluminescence and plasma display panel phosphors in the visible region. For example, the integration of ZnO with  $\text{SrAl}_2\text{O}_4$  rich in intrinsic defects may make it possible to achieve excellent PL properties. In addition, the strontium aluminate has also been used in the  $\text{Al}_2\text{O}_3$  matrix [16] to improve its mechanical properties such as strength and toughness due to the formation of anisotropic elongated grains [3].

$\text{SrAl}_2\text{O}_4$  has a tridymite structure. At ambient temperature, the stable  $\text{SrAl}_2\text{O}_4$  crystalline phase is monoclinic which transforms to hexagonal (an endothermic process) at a temperature of  $650^\circ\text{C}$ . Conversely, the reverse hexagonal–monoclinic transformation occurs (an exothermic process) at those temperatures [17].

With the development of scientific technologies on materials, several chemical synthesis methods such as sol-gel process [18], co-precipitation as well as combustion methods [19,20] and mechano-chemical reactions [21] have been applied to prepare  $\text{SrAl}_2\text{O}_4$ . All of these methods were conducted in liquid phases so that each component can be accurately controlled and uniformly mixed. However, expensive chemicals are consumed during preparation of  $\text{SrAl}_2\text{O}_4$  by the above-mentioned methods [22–24]. Commercial strontium aluminate powders are usually prepared by a solid-state reaction process [25] using expensive oxides as starting materials. Therefore, this work will focus on decreasing the cost of  $\text{SrAl}_2\text{O}_4$  preparation utilizing the alum sludge as an alumina source. However, the solid-state reaction needs high temperatures for preparation. The insufficient mixing and low reactivity of raw materials lead to several impurity phases such as  $\text{Al}_2\text{O}_3$ ,  $\text{SrO}$ , and other strontium aluminate phases that easily exist in the final products [26–28]. Therefore, optimizing the chemical reactions of the starting materials will be determined in this work in order to obtain stable  $\text{SrAl}_2\text{O}_4$ .

## 2. Material and methods

### 2.1. Alumina powder preparation

Alum sludge has been collected from the El-Manial water station (Giza – Egypt) and analyzed by X-ray fluorescence (XRF) [29]. The alum sludge was filtrated by a water suction pump to remove the water, followed by drying the slurries for 24 h at  $110^\circ\text{C}$ .

The method of  $\text{Al}(\text{OH})_3$  production from alum sludge is demonstrated previously by Khattab et al. [29] as follows: 50 mL of  $7 \text{ mol L}^{-1}$  sulfuric acid solution was added to 10 g of alum sludge. The mixture was stirred by a mechanical agitator at a rate of 300 rpm and heated at  $170^\circ\text{C}$  for 1 h. After that, 100 mL of distilled water was added into the flask and remained at room temperature overnight to extract soluble compounds from the resulting mixture. Next, the slurry was filtered followed by the slow addition of  $7.66 \text{ mol L}^{-1}$  of sodium hydroxide solution to the filtrate with a constant rate of  $3 \text{ mL min}^{-1}$  under a continuous stirring accompanied by adjusting alkalinity of medium to  $\text{pH} = 12$ . The flask was retained at room temperature over night for complete separation of total iron hydroxides " $\text{Fe}(\text{OH})_2$  &  $\text{Fe}(\text{OH})_3$ " from soluble  $\text{Al}^{3+}$  compounds and then the resulting slurry was filtrated. The produced solid components with reddish brown color were dried at  $100^\circ\text{C}$  for 24 h in an oven after

washing with distilled water. The filtrate was heated at  $70^\circ\text{C}$  and  $2.2 \text{ mol L}^{-1}$  ammonium acetate was added with a constant rate of  $3 \text{ mL min}^{-1}$  to re-precipitate  $\text{Al}(\text{OH})_3$  at  $\text{pH} = 8$ . The obtained precipitate was calcined for 2 h. at  $1,400^\circ\text{C}$  as demonstrated in our previous work [29].

### 2.2. Role of $\text{Sr}(\text{NO}_3)_2$ calcination

The  $\text{Sr}(\text{NO}_3)_2$  powders were purchased with extra purity 98% (CAS:10042-76-9) and were calcined at  $1,100^\circ\text{C}$  for 1 h at a rate of  $40^\circ\text{C min}^{-1}$ . The second calcination of  $\text{Sr}(\text{NO}_3)_2$  powders at  $1,100^\circ\text{C}$  was performed for 1 h at heating rate  $20^\circ\text{C min}^{-1}$  and named SR2. A third calcination at  $1,100^\circ\text{C}$  for 1 h at heating rate  $20^\circ\text{C min}^{-1}$  has been carried out for SR2 powders to obtain SR3 powders. The XRD characterization for both SR2 and SR3 are shown in Fig. 1. It is observed that the  $\text{Sr}(\text{OH})_2 \cdot \text{H}_2\text{O}$  is the main constituent for SR2.  $\text{Sr}(\text{OH})_2$  and  $\text{SrO}$  are the main constituents of SR3.

### 2.3. Batch preparations

Four mix powders were prepared after alumina calcinations at  $1,400^\circ\text{C}$ . The compositions of these mixes were based on stoichiometric calculations of  $\text{Sr}(\text{NO}_3)_2$ ,  $\text{Sr}(\text{OH})_2 \cdot \text{H}_2\text{O}$ ,  $\text{Sr}(\text{OH})_2$ , or  $\text{SrO}$  separately with alumina as the main compositions for  $\text{SrAl}_2\text{O}_4$  formation and called AS1, AS2, AS3 and AS4, respectively. For preparing AS1 powder,  $\text{Sr}(\text{NO}_3)_2$  was used without calcination to compare with the other mixes (AS2, AS3 and AS4). The four mix powders were then calcined at  $1,100^\circ\text{C}$  for 1 h. The calcined mix powders were subjected to a uniaxial pressing under pressure of 100 MPa and fired at different sintering temperatures:  $1,200^\circ\text{C}$ ,  $1,400^\circ\text{C}$  and  $1,500^\circ\text{C}$  to follow the change in the phase compositions. The optimum compositions were candidates for fired at  $1,550^\circ\text{C}$  and  $1,650^\circ\text{C}$  to show the effect of increasing the sintering temperature on the phase compositions and microstructure.

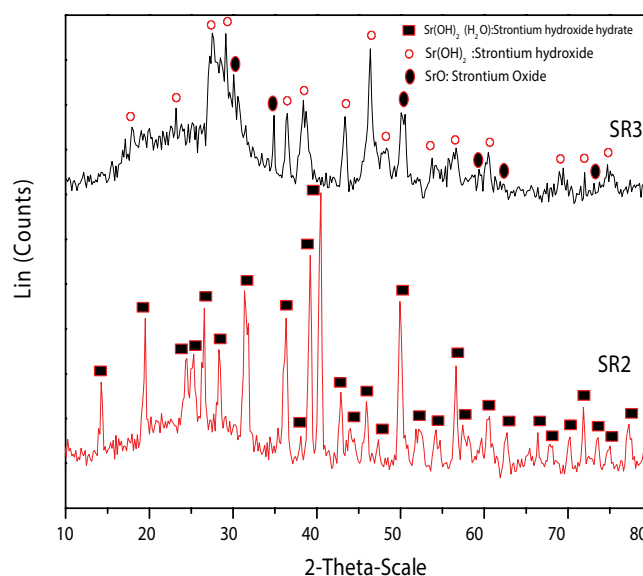


Fig. 1. XRD patterns of SR2 and SR3 calcined for 1 h at  $1,100^\circ\text{C}$ .

2.4. Characterization

X-ray diffractometer type Philips, model Bruker D8 Advance-Germany, target Cu K $\alpha$ , with secondary monochromator, V = 40 kv, A = 40 mA, and Ni filter was used to investigate the phase composition of SrAl<sub>2</sub>O<sub>4</sub>. The chemical compositions of alum sludge were characterized by XRF (Analytical 2005). The morphological characteristics of the batches were examined by SEM equipment (Philips XL 30) after coating with thin gold films. The bulk density and apparent porosity of the sintered samples were determined by Archimedes method. The compressive strength of sintered bodies was tested by using an automatic hydraulic testing machine (type Shimadzu Co. Kyoto, Japan of maximum capacity 1,000 kN by rate of 0.025 kN mm<sup>-2</sup>S<sup>-1</sup>).

3. Results and discussion

3.1. Phase compositions

Figs. 2–5 present the XRD patterns of the four calcined powders (AS1, AS2, AS3 and AS4) at 1,100°C and four sintered batches at 1,200°C, 1,400°C and 1,500°C, respectively. From Fig. 2 calcined AS3 powders showed the formation of SrAl<sub>2</sub>O<sub>4</sub> as the main phase with minor amounts of Sr<sub>3</sub>Al<sub>2</sub>O<sub>6</sub>. For AS1 and AS4 powders, the Sr<sub>3</sub>Al<sub>2</sub>O<sub>6</sub> is the main phase with presence of small amount SrAl<sub>2</sub>O<sub>4</sub>. Major phase of Sr<sub>3</sub>Al<sub>2</sub>O<sub>6</sub> was obtained for AS2 powder after calcining at 1,100°C. The combination of SrAl<sub>2</sub>O<sub>4</sub> and Sr<sub>3</sub>Al<sub>2</sub>O<sub>6</sub> phases of the sintered samples at 1,200°C was observed (Fig. 3). The peaks of (011), (211), (220), (211) and (031) planes indicated the presence of SrAl<sub>2</sub>O<sub>4</sub> crystal [30]. For AS1 and AS4 batches, it is observed that the main peaks are SrAl<sub>2</sub>O<sub>4</sub> phase after sintering at 1,400°C and 1,500°C. In addition, there are other peaks; SrAl<sub>12</sub>O<sub>19</sub> and alumina, observed besides SrAl<sub>2</sub>O<sub>4</sub> phase for AS4 batch and minor amounts of alumina and Sr<sub>3</sub>Al<sub>2</sub>O<sub>6</sub> for AS1 batches after sintering at 1,400°C and 1,500°C. The intensity of SrAl<sub>2</sub>O<sub>4</sub> for AS4 batch is more than

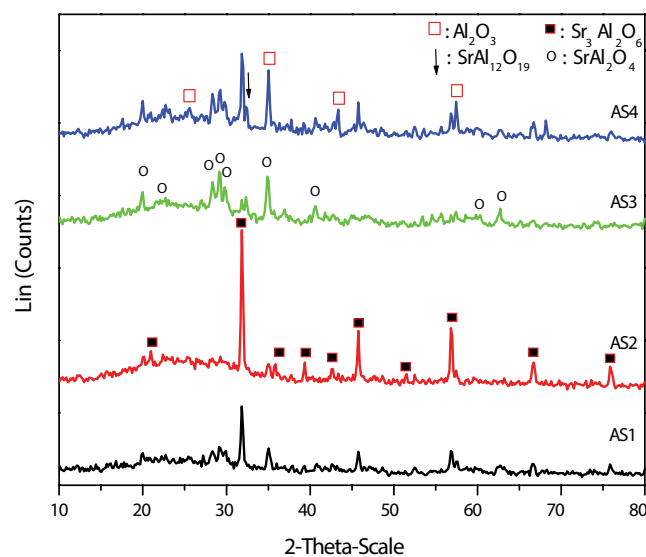


Fig. 2. XRD patterns of AS1, AS2, AS3 and AS4 calcined powders for 1 h at 1,100°C.

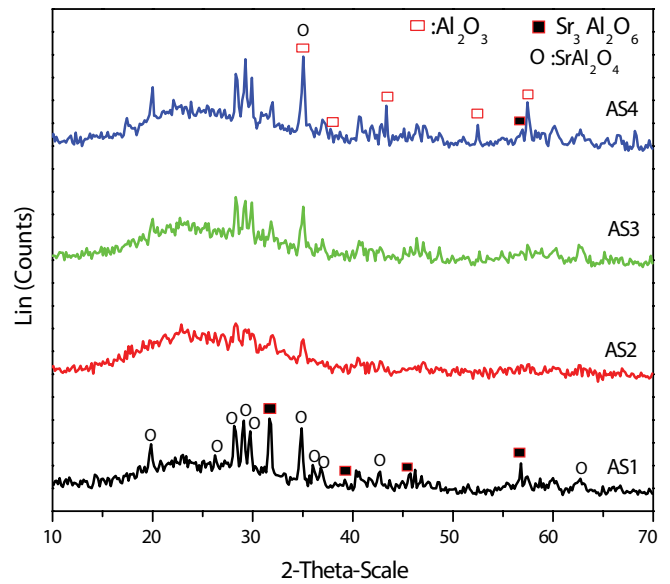


Fig. 3. XRD patterns of calcined AS1, AS2, AS3 and AS4 batches sintered for 1 h at 1,200°C.

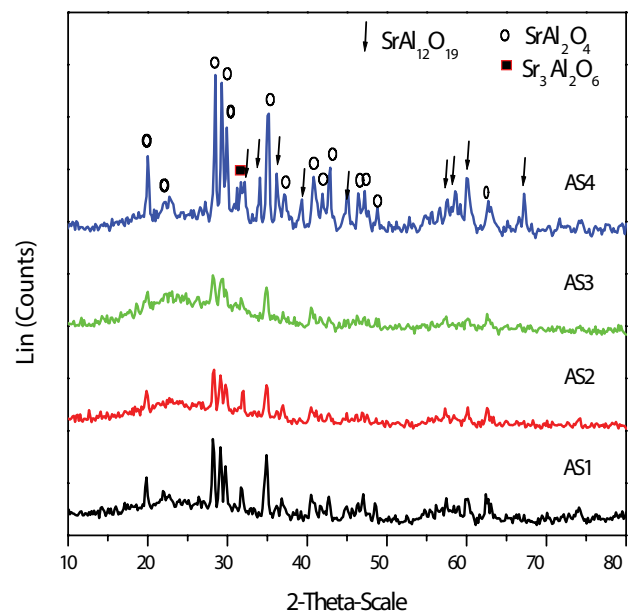


Fig. 4. XRD patterns of calcined AS1, AS2, AS3 and AS4 batches sintered for 1 h at 1,400°C.

AS1. On the contrary, for AS2 and AS3 batches at 1,400°C, there is an increase in the peak intensities of Sr<sub>3</sub>Al<sub>2</sub>O<sub>6</sub> phase during the formation of SrAl<sub>2</sub>O<sub>4</sub> phase. This result can be explained as follows: during the first stage of the calcination at 1,100°C, thermal decompositions of Sr(NO<sub>3</sub>)<sub>2</sub> for AS1 batches, Sr(OH)<sub>2</sub>OH for AS2 batches, Sr(OH)<sub>2</sub> for AS3 and AS4 batches happened, which initiate the chemical reaction between SrO and Al<sub>2</sub>O<sub>3</sub>. Immediately, the nucleation and growth of Sr<sub>3</sub>Al<sub>2</sub>O<sub>6</sub> particles occur as seen in Eq. (1) [31].



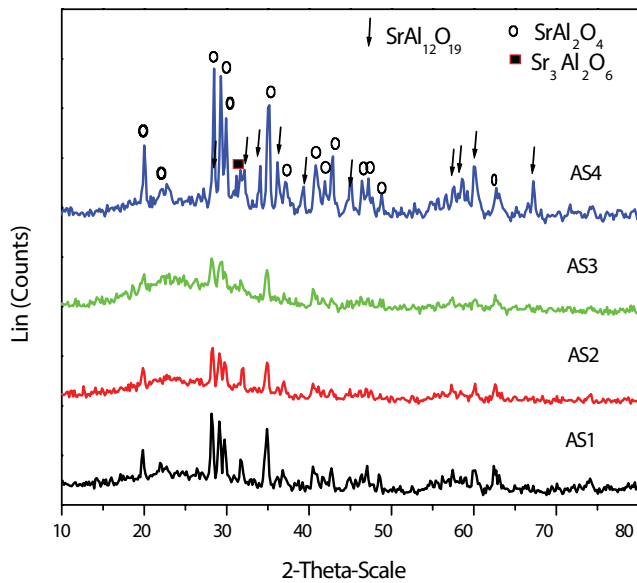
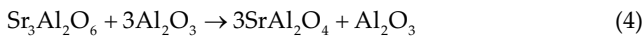


Fig. 5. XRD patterns of calcined AS1, AS2, AS3 and AS4 batches sintered for 1 h at 1,500°C.

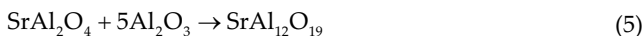
After sintering the samples at 1,200°C, the residual SrO reacts with  $\text{Al}_2\text{O}_3$  and form the stable  $\text{SrAl}_2\text{O}_4$  phase beside the  $\text{Sr}_3\text{Al}_2\text{O}_6$  phase Eq. (2) [32].



The  $\text{Sr}_3\text{Al}_2\text{O}_6$  is transformed into  $\text{SrAl}_2\text{O}_4$  after sintering at 1,400°C (as seen in AS1 batches). However, in the presence of remaining excess of SrO and  $\text{Al}_2\text{O}_3$ , a reaction between part of  $\text{SrAl}_2\text{O}_4$  and SrO is occurred to form  $\text{Sr}_3\text{Al}_2\text{O}_6$  again as in the case of AS3 batches according to Eq. (3) [33]. This result is confirmed by decreasing of  $\text{SrAl}_2\text{O}_4$  intensity. Then, part of  $\text{Sr}_3\text{Al}_2\text{O}_6$  react with  $\text{Al}_2\text{O}_3$  to  $\text{SrAl}_2\text{O}_4$  according to Eq. (4) as indicated later at 1,500°C for AS3 batch.



On the contrary, in case of the presence of a very excess amount of  $\text{Al}_2\text{O}_3$  and sintering above 1,250°C, some peaks of new  $\text{SrAl}_{12}\text{O}_{19}$  phase were identified as seen in AS4 batches, according to Eq. (5) [34].



From the above, it was observed that AS4 batches are the optimum composition for the formation of high peak intensity of  $\text{SrAl}_2\text{O}_4$ . In general, the formation of high peak intensity of  $\text{SrAl}_2\text{O}_4$  for the AS4 batch rather than the AS1 batch can be explained by the direct reaction of SrO and  $\text{Al}_2\text{O}_3$ , which facilitates the formation of  $\text{SrAl}_2\text{O}_4$  later. On the contrary, for the AS1 batch, the decomposition of  $\text{Sr}(\text{NO}_3)_2$  occurred first to form SrO then the reaction with alumina to form  $\text{SrAl}_2\text{O}_4$  is performed.

For all the samples, AS1, AS2, AS3 and AS4 sintered at 1,500°C (Fig. 5) and for AS4 sintered at 1,550°C and 1,650°C (Fig. 6), a decrease in the intensity of the main phases is observed. These results can be explained by the formation of the liquid phase between  $\text{Sr}_3\text{Al}_2\text{O}_6$  and  $\text{SrAl}_2\text{O}_4$  phases at the eutectic point equaling 1,505°C according to the binary phase diagram  $\text{Al}_2\text{O}_3$ - $\text{SrO}_2$  system as seen in Fig. 7 [35].

### 3.2. DTA and TGA analysis

The DTA and TGA profiles are summarized and shown in Figs. 8 and 9 for two powder compositions; one composed of  $\text{Sr}(\text{NO}_3)_2$  and  $\text{Al}_2\text{O}_3$  powders, named PSA (Fig. 8) and the

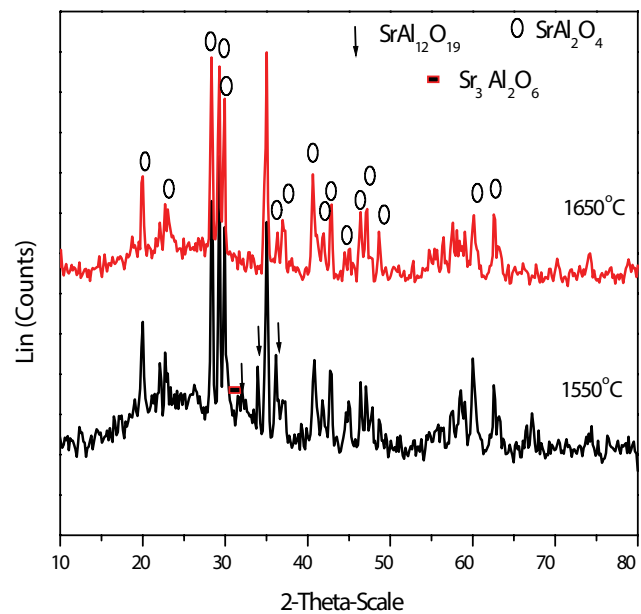


Fig. 6. XRD patterns of AS4 sample sintered for 1 h at 1,550°C and 1,650°C.

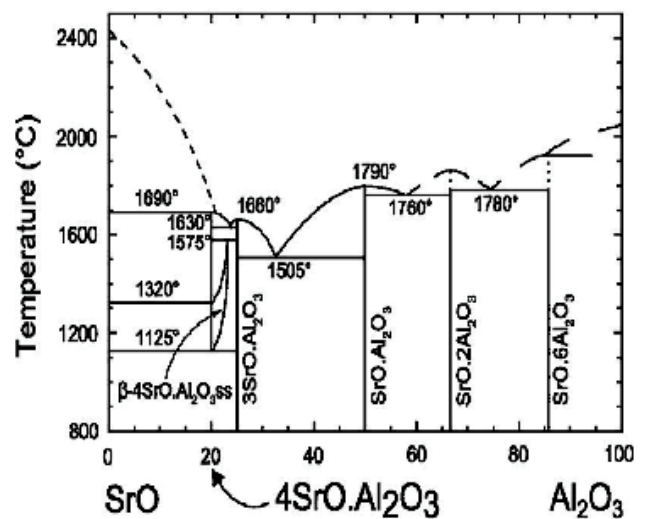


Fig. 7. Phase diagram of SrO- $\text{Al}_2\text{O}_3$  system [35].

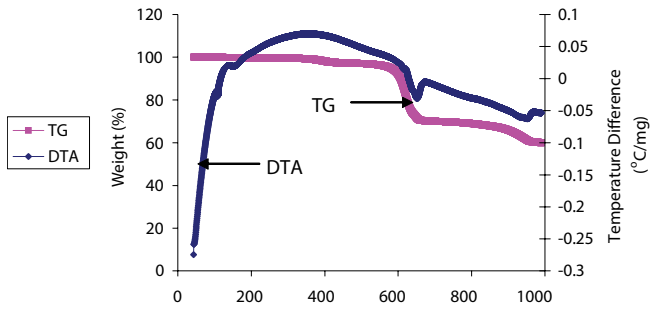


Fig. 8. DTA and TGA thermograms of PSA ( $\text{Sr}(\text{NO}_3)_2$  and  $\text{Al}_2\text{O}_3$ ) powders.

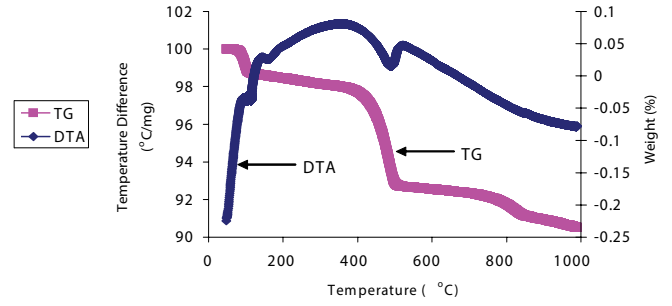
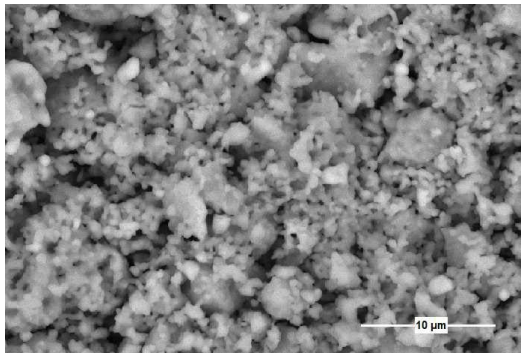
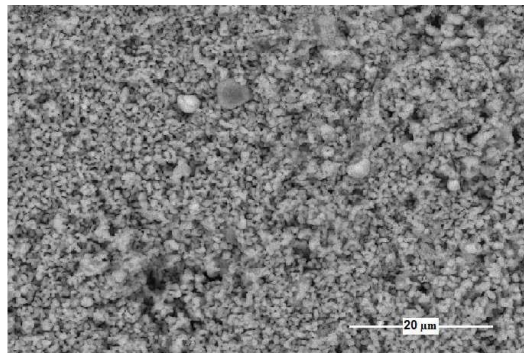


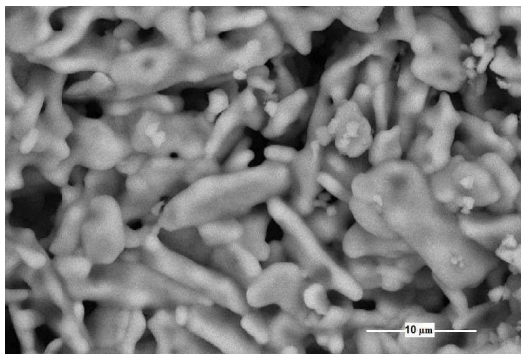
Fig. 9. DTA and TGA thermograms of CSA (SR3 " $\text{SrO} + \text{Sr}(\text{OH})_2$ " and  $\text{Al}_2\text{O}_3$ ) powders.



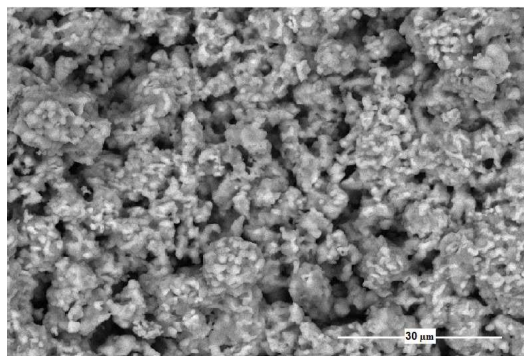
AS1, 1200 °C



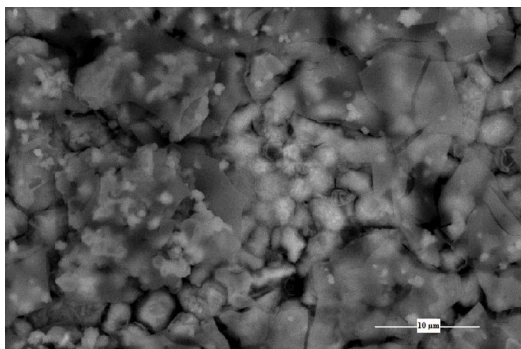
AS2, 1200 °C



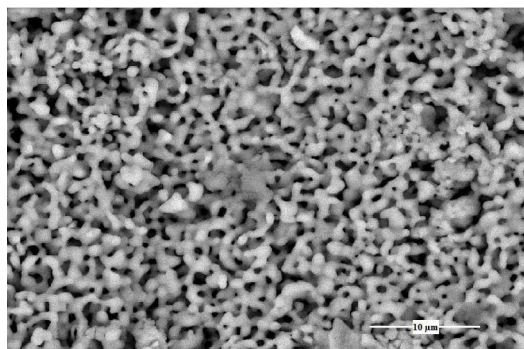
AS1, 1400 °C



AS2, 1400 °C



AS1, 1500 °C



AS2, 1500 °C

Fig. 10. SEM micrographs of AS1 and AS2 batches after sintering for 1 h at 1,200°C, 1,400°C and 1,500°C.

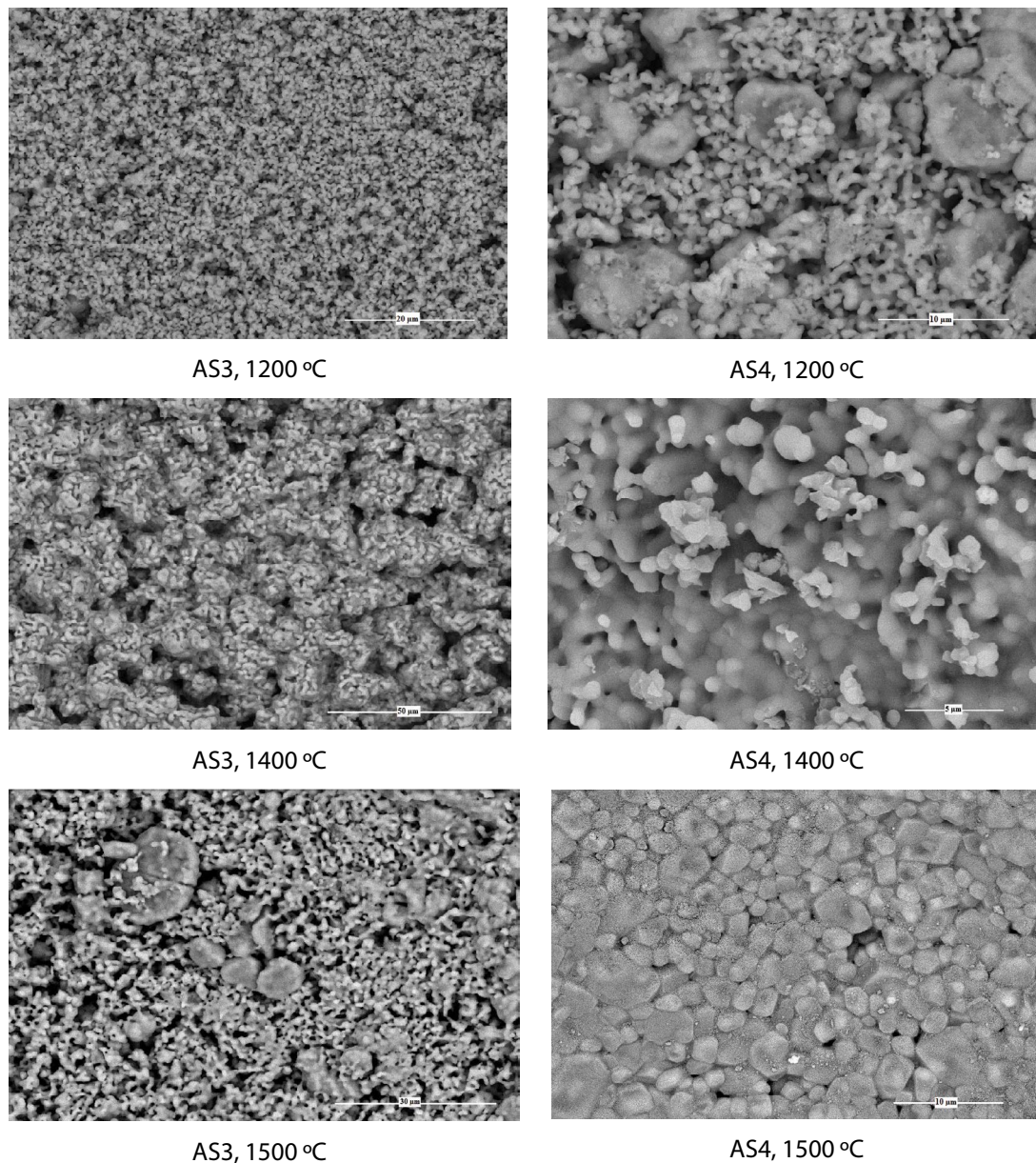


Fig. 11. SEM micrographs of AS3 and AS4 batches after sintering for 1 h at 1,200°C, 1,400°C and 1,500°C.

other composition composed of SR3 ( $\text{SrO} + \text{Sr}(\text{OH})_2$ ) and  $\text{Al}_2\text{O}_3$  powders, named CSA (Fig. 9). For the PSA composition, the evaporation of absorbed water was observed by the appearance of one endothermic peak in the range of 80°C–250°C. The decomposition of  $\text{NO}_3$  group occurred gradually with the formation of an endothermic peak at 620.73°C accompanied by weight loss of about 29.85% and another peak appeared at 946.37°C with weight loss of about 10.17%. In case of CSA composition, the evaporation of absorbed water is observed in two endothermic peaks at about of 113°C and 163°C accompanied by weight loss of 2.046%. Furthermore, there is an apparent endothermic peak at 487°C that could probably be attributed to the dissociation of  $\text{Sr}(\text{OH})_2$  in SR3 powder with weight loss of about 5.695%. At higher temperature (above 800°C), a broad and partially thermal stability in

the range of 800°C–1,000°C in the TGA profile was explained by the starting formation of the  $\text{SrAl}_2\text{O}_4$  phase.

### 3.3. SEM analysis

Figs. 10 and 11 show a high magnification of SEM micrographs of AS1, AS2, AS3 and AS4 batches after sintering at 1,200°C, 1,400°C and 1,500°C for 1 h. It is observed that as the sintering temperature increased, the particle size increased. For AS1 samples (Fig. 10), it is shown that an evidence of the clustered nanoparticle matrix was appeared at 1,200°C referred to  $\text{Sr}_3\text{Al}_2\text{O}_6$  (white area) and contained bulk grains in form of plated shapes referred to  $\text{SrAl}_2\text{O}_4$  (gray area). Upon increasing the sintering temperature to 1,400°C and 1,500°C, the increasing in the bulk plated grains

( $\text{SrAl}_2\text{O}_4$ ) is observed containing minor amounts of  $\text{Sr}_3\text{Al}_2\text{O}_6$  in the form of small spherical particles. For AS2 and AS3 batches sintered at  $1,200^\circ\text{C}$  (Figs. 10 and 11), it was observed that the matrix has small agglomerated light sphere particle shapes that indicated  $\text{Sr}_3\text{Al}_2\text{O}_6$  with gray small particles refer to  $\text{SrAl}_2\text{O}_4$ . By increasing the sintering temperature to  $1,400^\circ\text{C}$ , both batches showed the  $\text{SrAl}_2\text{O}_4$  embedded (cubic shapes) within the  $\text{Sr}_3\text{Al}_2\text{O}_6$  matrix. As shown in AS2 and AS3 batches, it observed that the bulk grains of  $\text{SrAl}_2\text{O}_4$  were transformed into  $\text{Sr}_3\text{Al}_2\text{O}_6$  (small sphere shapes). Upon increasing the temperature to  $1,500^\circ\text{C}$ , the partial formation of liquid phases is observed [35]. In case of AS4 batch, both phases of strontium aluminate, that is,  $\text{Sr}_3\text{Al}_2\text{O}_6$  in the form of small sphere shapes and  $\text{SrAl}_2\text{O}_4$  in the form of sheet shapes, are formed after sintering at  $1,200^\circ\text{C}$  (Fig. 10). By increasing the sintering temperature to  $1,400^\circ\text{C}$  and  $1,500^\circ\text{C}$ , the matrix contains mainly  $\text{SrAl}_2\text{O}_4$  phases for AS4 batch as seen in Fig. 11. However, AS1 and AS4 batches presented the incipient formation of necks in the particles contact points at  $1,400^\circ\text{C}$  which reverse on the grain growth of  $\text{SrAl}_2\text{O}_4$  particles at  $1,500^\circ\text{C}$ . For AS4 batch at  $1,550^\circ\text{C}$  and  $1,650^\circ\text{C}$  (Fig. 12), the partial fusion of batches and formation of liquid phase is observed.

### 3.4. Physical properties

The apparent porosity and bulk density for samples AS1, AS2, AS3 and AS4 after sintering at  $1,400^\circ\text{C}$  and  $1,500^\circ\text{C}$  are shown in Figs. 13 and 14, respectively. It was observed the apparent porosity decreases and bulk density increases with increasing the sintering temperature. This is due to the solid-state reaction and phase's development [36]. AS2 and AS3 showed an increase in the porosity amounts compared with AS1 and AS4 samples. These behaviors are related to large exhausted gases from these batches due to gradual dissociation of  $\text{Sr}(\text{OH})_2\text{OH}$  for SR2 composition and dissociation of  $\text{Sr}(\text{OH})_2$  for SR3 composition. As mentioned above, according to TGA and DTA results, the AS3 batch has more ability to absorb water than AS1 batch, which affects on the apparent porosity values. The bulk density increases by increasing the sintering temperature due to the formation of interlocked crystals that lead to body compactions [37–40]. In other words, a large number of contact points are formed among the particles resulting shorter diffusion paths. This in turn increases

the average coordination number of particles and leads to an enhancement in sinterability [41]. It is found that AS1 and AS4 batches showed higher bulk densities than AS2 and AS3 batches. By increasing the sintering temperature at  $1,500^\circ\text{C}$ ,

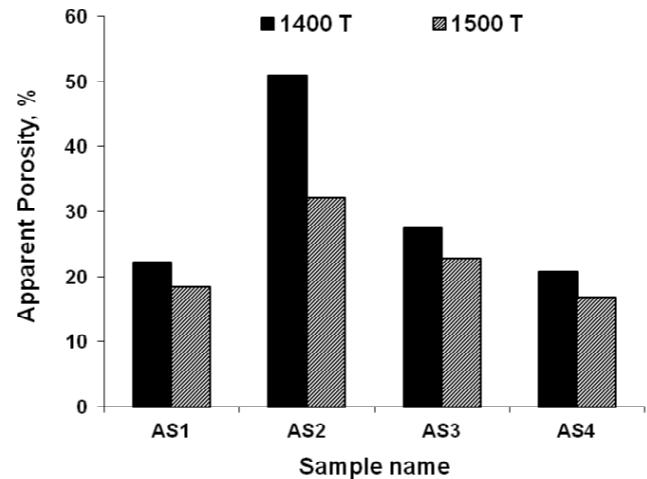


Fig. 13. Apparent porosity of AS1, AS2, AS3 and AS4 samples after sintering for 1 h at  $1,400^\circ\text{C}$  and  $1,500^\circ\text{C}$ .

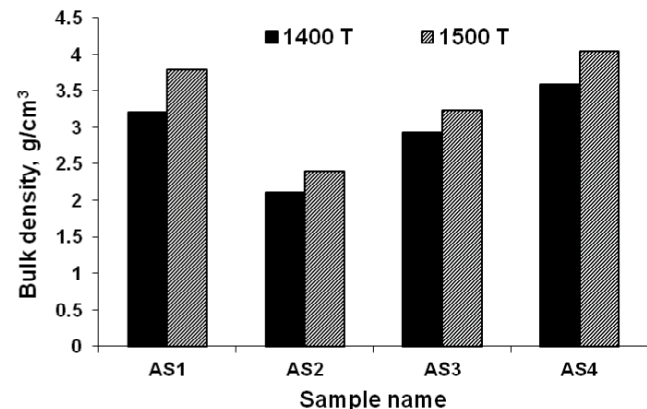
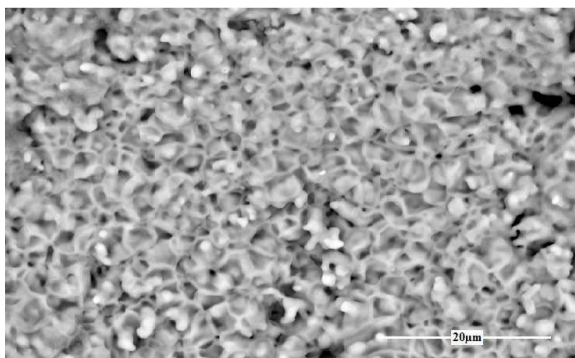
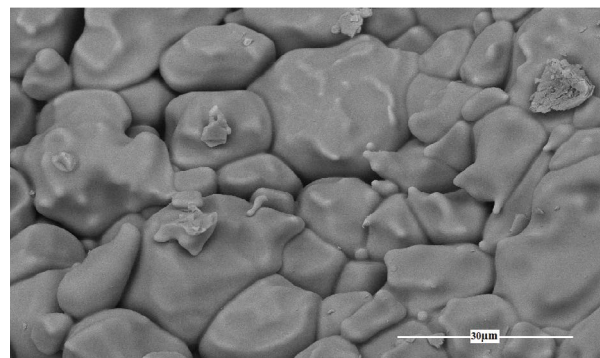


Fig. 14. Bulk density of AS1, AS2, AS3 and AS4 samples after sintering for 1 h at  $1,400^\circ\text{C}$  and  $1,500^\circ\text{C}$ .



AS4,  $1550^\circ\text{C}$



AS4,  $1650^\circ\text{C}$

Fig. 12. SEM micrographs of AS4 batch after sintering for 1 h at  $1,550^\circ\text{C}$  and  $1,650^\circ\text{C}$ .

which refers to an increase in the number of contact points between the particles and partially solubility of  $\text{Sr}_3\text{Al}_2\text{O}_6$  phase between particles, that fills most of the open pores between the spinel grains and enhances the body compactions.

For the optimum composition AS4 batch (Figs. 15a and b), it was observed an enhancement in apparent porosity and bulk density after sintering at 1,550°C, then the decreasing in the sinterability parameters is estimated at 1,650°C, that is, an increase in porosity and a decrease in density. This is due to the formation of in situ liquid phase that makes distortion and bloating for the grain boundaries resulted in the presence of isolated pores [35].

### 3.5. Mechanical properties

The compressive strength for four batch compositions of AS1, AS2, AS3 and AS4 after sintering at different temperatures 1,400°C and 1,500°C and for optimum composition AS4 sintered at 1,550°C and 1,650°C are shown in Figs. 16 and 17, respectively. It was observed that an improvement in strength for AS4 and AS1 batches at 1,500°C and 1,400°C compared with AS2 and AS3 batches. The degradation of strength values for AS2 and AS3 is due to the presence of pores in the sintered specimens. Thus, for increasing the strength, the body becomes high dense with low porosity [16]. Fig. 17 also shows an enhancement of strength occurred for AS4 sintered at 1,550°C in comparable with sintering at 1,400°C

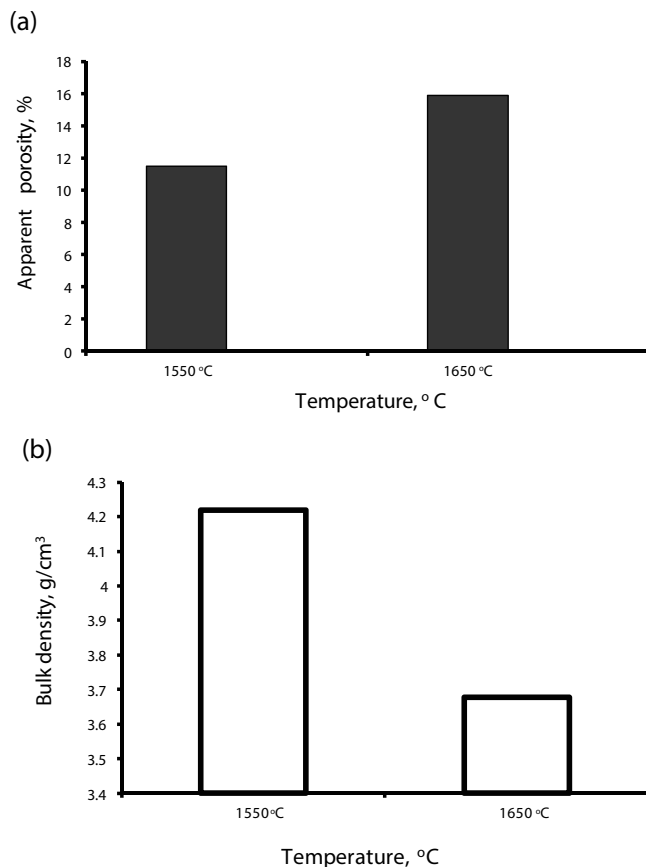


Fig. 15. (a) Apparent porosity and (b) bulk density of AS4 sample after sintering for 1 h at 1,550°C and 1,650°C.

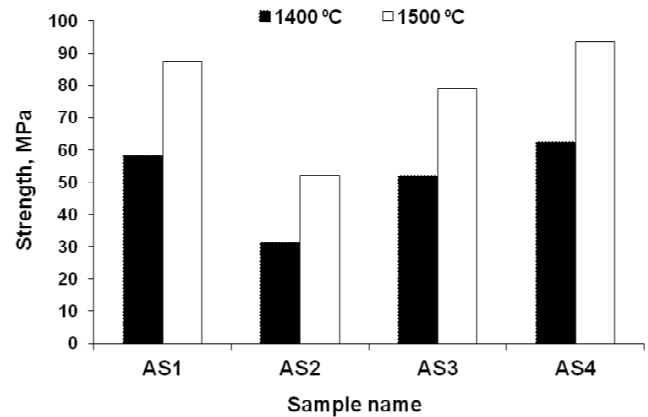


Fig. 16. Compressive strength of AS1, AS2, AS3 and AS4 sample after sintering for 1 h at 1,400°C and 1,500°C.

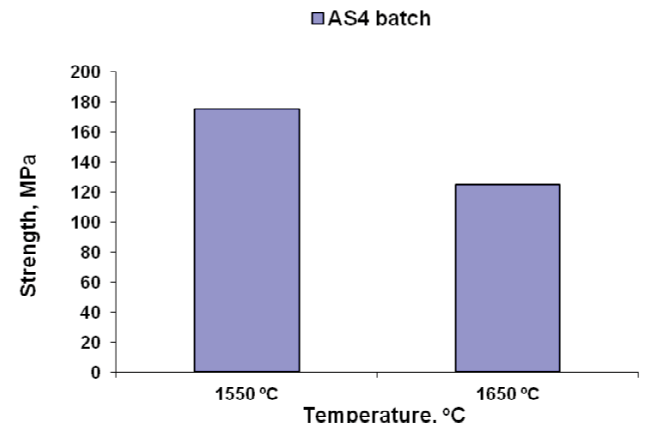


Fig. 17. Compressive strength of AS4 sample after sintering for 1 h at 1,550°C and 1,650°C.

and 1,500°C. The decreasing in strength was obtained of AS4 batch after sintering at 1,650°C due to the formation of high amounts of liquid phase as seen in SEM.

### 4. Conclusion

The present work succeeded in preparation of strontium aluminate ( $\text{SrO} \cdot \text{Al}_2\text{O}_3$ ) by using strontium nitrate and alumina recycled from alum sludge after it is calcined at 1,400°C. The research work based on utilizing parts of strontium nitrate without subjecting to calcination and other parts were subjected to calcination at 1,100°C for 1 h at heating rate 40°C min<sup>-1</sup>. The research work based on utilizing parts of strontium nitrate without subjecting to calcination and other parts were subjected to calcination at 1,100°C for 1 h at heating rate 40°C min<sup>-1</sup>. The calcined strontium nitrate powders are divided into two parts. Part of it is calcined at 1,100°C for 1 h at heating rate 20°C min<sup>-1</sup> and another part is calcined at 1,100°C for 2 h at heating rate 20°C min<sup>-1</sup>. According to the phase compositions, four stoichiometric calculation was performed for  $\text{Sr}(\text{NO}_3)_2$ ,  $\text{Sr}(\text{OH})_2$ ,  $\text{Sr}(\text{OH})_2 \cdot \text{H}_2\text{O}$  and SrO separately with alumina to follow the phase compositions of  $\text{SrAl}_2\text{O}_4$ . The mixed powders were dried and calcined at

1,100°C, then compacted and sintered at 1,200°C, 1,400°C and 1,500°C. After that, the optimization of the batches was selected according to the amount of SrAl<sub>2</sub>O<sub>4</sub>. The optimized batch was selected according to the amount of SrAl<sub>2</sub>O<sub>4</sub> and sintered at 1,550°C and 1,650°C. The results indicated that the composition that was calculated according to SrO contents exhibited good physical and mechanical properties at 1,550°C. This is due to the direct reaction between SrO and Al<sub>2</sub>O<sub>3</sub>, which enhances the formation of the high amount of SrAl<sub>2</sub>O<sub>4</sub> early. Therefore, this work is succeeded to prepare SrAl<sub>2</sub>O<sub>4</sub> that could be used in advanced ceramic applications, aluminous hydraulic binder materials as special inorganic cements, host materials for PL, cathode luminescence and plasma display panel phosphors in visible region.

### Acknowledgment

The team would like to thank the National Research Centre which supports the present work through the project No. 11070203.

### References

- [1] M.B. Khalid, G.F. Faris, M.A. Isam, Reuse of alum sludge in construction materials and concrete works: a general overview, *Infrastruct. Univ. Kuala Lumpur Res. J.*, 2 (2014) 20–30.
- [2] Y.W. Ling, S. Dong, Z. Li, G.L. Feng, A. Ning, H.Y. Wei, H.Z. Chun, Utilization of alum sludge for producing aluminum hydroxide and layered double hydroxide, *Ceram. Int.*, 40 (2014) 15503–15514.
- [3] M. Manali, Preparation and Characterization of Alumina-Strontium Aluminate Based Composite, Thesis, National Institute of Technology, Roukela, 2015.
- [4] R.C. Ropp, *Encyclopedia of the Alkaline Earth Compounds*, Elsevier, Amsterdam, 2013.
- [5] P. Ptáček, F. Šoukal, T. Opravil, E. Bartoníčková, M. Zmrzlý, R. Novotný, Synthesis, hydration and thermal stability of hydrates in strontium-aluminate cement, *Ceram. Int.*, 40 (2014) 9971–9979.
- [6] M. Martynas, J. Jens-Erik, K. Aivaras, Sol-gel synthesis, structural and optical properties of cerium-doped strontium aluminates, Sr<sub>3</sub>Al<sub>2</sub>O<sub>6</sub> and SrAl<sub>12</sub>O<sub>19</sub>, *Mater. Sci.*, 19 (2013) 438–442.
- [7] P. Ptáček, *Strontium Aluminate - Cement Fundamentals, Manufacturing, Hydration, Setting Behaviour and Applications*, 2014, Available at doi: 10.5772/57363, ISBN: 978-953-51-1591-5.
- [8] I. Odler, *Special Inorganic Cements (Modern Concrete Technology)*, 1st Ed., Taylor & Francis Group, New York, 2000.
- [9] N. Illyouka, V. Timofeeva, *Development of Hydraulic Zirconia Cements and Their Applications for Productions of Refractories Items*, T.t. University (Ed.), Kharkov, Ukraine, 1998.
- [10] A. Douy, M. Capron, Crystallisation of spray-dried amorphous precursors in the SrO–Al<sub>2</sub>O<sub>3</sub> system: a DSC study, *J. Eur. Ceram. Soc.*, 23 (2003) 2075–2081.
- [11] A.K. Chatterjee, Re-examining the prospects of aluminous cements based on alkali-earth and rare-earth oxides, *Cem. Concr. Res.*, 39 (2009) 981–988.
- [12] K. Bum-Joon, H. Zubair, K. Jung-Sik, Synthesis and characterization of long persistence Sr<sub>4</sub>Al<sub>14</sub>O<sub>25</sub>: Eu<sup>2+</sup>, Dy<sup>3+</sup> phosphor prepared by combustion method, *Int. J. Ceram. Process. Res.*, 14 (2013) 601–605.
- [13] G.I. Akmeahmet, S. Šturm, L. Bocher, M. Kociak, B. Ambrožič, C.W. Ow-Yang, Structure and luminescence in long persistence Eu, Dy, and B codoped strontium aluminate phosphors: the boron effect, *J. Am. Ceram. Soc.*, 99 (2016) 2175–2180.
- [14] D. Haranath, S. Virendra, C. Harish, S. Pooja, Tuning of emission colours in strontium aluminate long persisting phosphor, *J. Phys. D: Appl. Phys.*, 36 (2003) 2244–2248.
- [15] M. Avdeev, S. Yakovlev, A.A. Yaremchenko, V.V. Kharton, Transitions between P21, P63 and P6322 modifications of SrAl<sub>2</sub>O<sub>4</sub> by *in situ* high-temperature X-ray and neutron diffraction, *J. Solid State Chem.*, 180 (2007) 3535–3544.
- [16] V.P. Singh, A.P. Mohanty, A.S.P. Lochab, R. Chandana, Anomalous luminescent properties in ZnO and SrAl<sub>2</sub>O<sub>4</sub> composites, *RSC Adv.*, 4 (2014) 36765–36770.
- [17] C. Yu-Lun, H. Hsing-I, Phase evolution during formation of SrAl<sub>2</sub>O<sub>4</sub> from SrCO<sub>3</sub> and α-Al<sub>2</sub>O<sub>3</sub>/AlOOH, *J. Am. Ceram. Soc.*, 90 (2007) 2759–2765.
- [18] M. Misevicius, O. Scit, I. Grigoraviciute-Puroniene, G. Degutis, I. Bogdanoviciene, A. Kareiva, Sol-gel synthesis and investigation of un-doped and Ce-doped strontium aluminates, *Ceram. Int.*, 38 (2012) 5915–5924.
- [19] Z. Xue, S. Deng, Y. Liu, B. Lei, Y. Xiao, M. Zheng, Synthesis and luminescence properties of SrAl<sub>2</sub>O<sub>4</sub>: Eu<sup>2+</sup>/Dy<sup>3+</sup> hollow microspheres via a solvothermal co-precipitation method, *J. Rare Earths*, 31 (2013) 241–246.
- [20] H. Song, D. Chen, W. Tang, Y. Peng, Synthesis of SrAl<sub>2</sub>O<sub>4</sub>: Eu<sup>2+</sup>, Dy<sup>3+</sup>, Gd<sup>3+</sup> phosphor by combustion method and its phosphorescence properties, *Displays*, 29 (2008) 41–44.
- [21] N. Setoudeh, N.J. Welham, Ball milling induced reduction of SrSO<sub>4</sub> by Al, *Int. J. Miner. Process.*, 98 (2011) 214–218.
- [22] Y. Liu, C.N. Xu, Influence of calcining temperature on photoluminescence and triboluminescence of europium-doped strontium aluminate particles prepared by Sol-Gel process, *J. Phys. Chem. B*, 107 (2003) 3991–3995.
- [23] Z. Fu, S. Zhou, S. Zhang, Study on optical properties of rare-earth ions in nanocrystalline monoclinic SrAl<sub>2</sub>O<sub>4</sub>: Ln (Ln = Ce<sup>3+</sup>, Pr<sup>3+</sup>, Tb<sup>3+</sup>), *J. Phys. Chem. B*, 109 (2005) 14396–14400.
- [24] Y. Xu, W. Peng, S. Wang, X. Xiang, P. Lu, Synthesis of SrAl<sub>2</sub>O<sub>4</sub> and SrAl<sub>12</sub>O<sub>19</sub> via ethylenediaminetetraacetic acid precursor, *Mater. Chem. Phys.*, 98 (2006) 51–54.
- [25] Y.-L. Chang, H.-I. Hsiang, M.-T. Liang, F.-S. Yen, Phase evolution and thermal behaviors of the solid-state reaction between SrCO<sub>3</sub> and Al<sub>2</sub>O<sub>3</sub> to form SrAl<sub>2</sub>O<sub>4</sub> under air and CO<sub>2</sub>-air atmospheres, *Ceram. Int.*, 38 (2012) 2269–2276.
- [26] T. Peng, H. Yang, X. Pu, B. Hu, Z. Jiang, C. Yan, Combustion synthesis and photoluminescence of SrAl<sub>2</sub>O<sub>4</sub>: Eu, Dy phosphor nanoparticles, *Mater. Lett.*, 58 (2004) 352–356.
- [27] T. Aitasalo, P. Deren, J. Holsa, H. Jungner, J.C. Krupa, M. Lastusaari, J. Legendziewicz, J. Niittykoski, W. Strek, Persistent luminescence phenomena in materials doped with rare earth ions, *J. Solid State Chem.*, 171 (2003) 114–122.
- [28] J. Hölsä, H. Jungner, M. Lastusaari, J. Niittykoski, Persistent luminescence of Eu<sup>2+</sup> doped alkaline earth aluminates, MA<sub>2</sub>O<sub>4</sub>: Eu<sup>2+</sup>, *J. Alloys Compd.*, 323–324 (2001) 326–330.
- [29] R.M. Khattab, H.A. Badr, H.H. Abo-Almaged, H.E.H. Sadek, Recycling of alum sludge for alpha Al<sub>2</sub>O<sub>3</sub> production using different chemical treatments, *Desal. Wat. Treat.*, 113 (2018) 148–159.
- [30] C. Harish, D. Haranath, S. Virendra, S. Pooja, Synthesis of nanocrystals of long persisting phosphor by modified combustion technique, *J. Cryst. Growth*, 271 (2004) 307–312.
- [31] C. Yu-Lun, I.H. Hsing, L. Ming-Tsai, Characterizations of Eu, Dy co-doped SrAl<sub>2</sub>O<sub>4</sub> phosphors prepared by the solid-state reaction with B<sub>2</sub>O<sub>3</sub> addition, *J. Alloys Compd.*, 461 (2008) 598–603.
- [32] R.S. Garcés, T.J. Torres, V.A. Flores, Synthesis of SrAl<sub>2</sub>O<sub>4</sub> and Sr<sub>3</sub>Al<sub>2</sub>O<sub>6</sub> at high temperature, starting from mechanically activated SrCO<sub>3</sub> and Al<sub>2</sub>O<sub>3</sub> in blends of 3:1 molar ratio, *Ceram. Int.*, 38 (2012) 889–894.
- [33] C. Cheng, C. Teng-Ming, Effect of host compositions on the afterglow properties of phosphorescent strontium aluminate phosphors derived from the sol-gel method, *J. Mater. Res.*, 16 (2001) 1293–1300.
- [34] C. Chengkang, Y. Zhaoxin, M. Dali, Eu<sup>2+</sup> activated long persistent strontium aluminate nano scaled phosphor prepared by precipitation method, *J. Alloys Compd.*, 415 (2006) 220–224.
- [35] M. Franco, System SrO–Al<sub>2</sub>O<sub>3</sub>, (1964) pp. 118; Fig. 294 in *Phase diagram for ceramics, Part I*, Edited by Levine EM, Robbins CR, McMurdie HF, The American Ceramic Society; Ohio. &

- Massazza F., The system SrO–Al<sub>2</sub>O<sub>3</sub>, *Chim. Ind. (Milan)*, 41 (1959)108–115.
- [36] R.M. Khattab, M.M. El-Sayed Seleman, M.F. Zawrah, Assessment of electric arc furnace dust: Powder characterization and its sinterability as ceramic product, *Ceram. Int.*, 43 (2017) 12939–12947.
- [37] R.M. Khattab, M.M.S. Wahsh, N.M. Khalil, Ceramic compositions based on nano forsterite/nano magnesium aluminate spinel powders, *Mater. Chem. Phys.*, 166 (2015) 82–86.
- [38] R.M. Khattab, M.M.S. Wahsh, N.M. Khalil, F. Gouraud, M. Huger, T. Chotard, Effect of nanospinel additions on the sintering of magnesia-zirconia ceramic composites, *ACS Appl. Mater. Interfaces*, 6 (2014) 3320–3324.
- [39] K. Alessio, L. Hagemann, Behaviour of refractory products under constant and varying cyclic stress, *Stahl-Eisen*, 11 (1990) 95–110.
- [40] G. Routschka, C. Woehrmeyer, F. Gebhardt, Studies on the behaviour of magnesia, spinel and forsterite refractory bricks under simulated service conditions in the middle regions of oil-fired glass furnace regenerators. Part 1. Corrosion tests and hot-mechanical behaviour of the test brick, *Glastech-Ber.*, 63 (1990) 87–92.
- [41] M.M.S. Wahsh, R.M. Khattab, M.F. Zawrah, Sintering and technological properties of alumina/zirconia/nano-TiO<sub>2</sub> ceramic composites, *Mater. Res. Bull.*, 48 (2013) 1411–1414.